Laser Profilometry to measure the bed evolution in a dam-break flow

ROBIN MEURICE, PhD. Student, *Institute of Mechanics, Materials and Civil Engineering, Université Catholique de Louvain, Louvain-la-Neuve, Belgium*

Email: robin.meurice@uclouvain.be

SERGIO MARTÍNEZ-ARANDA, PhD, *Fluid Mechanics-I3A, University of Zaragoza, Spain*

Email: sermar@unizar.es

MASOUMEH EBRAHIMI, PhD Student, *Institute of Mechanics, Materials and Civil Engineering, Université Catholique de Louvain, Louvain-la-Neuve, Belgium*

Email: masoumeh.ebrahimi@uclouvain.be

PILAR GARCÍA-NAVARRO, Professor, *Fluid Mechanics-I3A, University of Zaragoza, Spain*

Email: pigar@unizar.es

SANDRA SOARES-FRAZÃO (IAHR Member), Professor, *Institute of Mechanics, Materials and Civil Engineering, Université Catholique de Louvain, Louvain-la-Neuve, Belgium*

Email: sandra.soares-frazao@uclouvain.be (author for correspondence)

Running Head: Laser Profilometry measurements of bed evolution.

Laser Profilometry to measure the bed evolution in a dam-break flow

ABSTRACT

A Laser Profilometry Technique was upgraded to detect underwater bed level evolution with a laser and a single camera for highly transient laboratory experiments. While being very simple, the proposed procedure achieves a similar performance as that met by more complex and expensive methods. This technique was applied to a dam-break test case over a mobile bed in a channel with a 90° bend, for which water and bed levels were both continuously recorded at five different places. Photogrammetry was then used to reconstruct the final topography, whose main features could be explained thanks to the analysis of only a few linear bed profiles appropriately chosen. This cheap, simple, flexible and yet accurate method thus proves to be an interesting alternative to more complex methods for morphodynamics investigations in the case of fast transient flows.

Keywords: Dam-break, laboratory studies, laser profilometry, morphodynamics, photogrammetry, sediment transport, transient flow.

1. **Introduction**

Bed dynamics detection under highly unsteady free-surface flows is one of the most challenging problems for experimental hydraulic researchers. Most of the time, two-dimensional (2D) unsteady surface flows are characterised by fast water surface and velocity evolutions, which produce rapid changes in the underlying erodible bed. Furthermore, these important variations in the bed elevation affect the flow dynamics as well. Because of the complex interaction between the flow and the bed dynamics, measuring the temporal evolution of the movable bed layer definitely requires to use non-intrusive optical techniques (Bouratsis et al., 2013). Nevertheless, optical access to the evolving bed is difficult to achieve, as well through the sidewalls of the channel if the bed evolution is two-dimensional, as through the fast-changing water surface. In particular, the optical distortion and aberrations created by the presence of a curved and turbulent air-water interface complicate the implementation of such techniques. However, this kind of 2D bed evolution data is necessary to calibrate and validate numerical models aimed at infrastructures design, restoration projects and hazard evaluation.

Despite the challenge, some experimental non-intrusive techniques have been reported in the last twenty years to detect the dynamics of the erodible bed at a laboratory scale.

A first family of techniques implies stopping the experiment when the measurements are to be taken, then draining the model and capturing the exposed bed regions (Aberle & Nikora, 2006; Butler et al., 1998; Carbonneau et al., 2003; Cooper & Tait, 2009; Dietrich et al., 1989; Goring et al., 1999). The bed topography and structure are then measured using different possible techniques (Bertin & Friedrich, 2014; Bunte & Abt, 2001). This methodology however requires that the morphological evolution is really stopped when the flow is interrupted. In addition, the combination of different experimental measurements at different times is not straightforward.

In the second family of techniques, the measurements of the bed evolution are taken during the flow, without stopping it. Among the different techniques available, photogrammetry emerges as the most widely developed one. Butler et al. (2002) first validated a stereo photographic system able to record the submerged bed dynamics in a laboratory flume, but the water-free surface had to be flattened by a transparent Perspex sheet for optical access to the bed. Henning et al. (2008) then used a 3D-photogrammetric laboratory setup to reconstruct the surface of both dry and submerged uniformly graded beds. They reported an accuracy close to 1 mm in the case of subcritical flow regimes and negligible disturbances of the water surface. Both studies only focused on steady water and bed situations, though. On the contrary, Bouratsis et al. (2013) applied a high-resolution photogrammetric technique to obtain measurements of a gravel bed bridge scour in a clear water flow. They used two partially submerged commercial cameras to record the evolution of the bed around the pier, and a set of computer vision and image processing algorithms to analyse the videos and reconstruct the instantaneous 3D surface of the bed. The required setup for this technique was relatively simple but intrusive. Frank and Hager (2014) applied 3D-photogrametry to measure the dike breaching process in a laboratory flume using four cameras and a grid projector. Even though these two last studies considered unsteady flows, their applicability to fast transient flows such as dam-break flows is uncertain, as it requires a sufficiently smooth free-surface. For example, the grid projected onto the dike by Frank and Hager (2014) could not be properly identified at the beginning of the breaching flow that they reproduced, because of a too irregular water free-surface. Smith et al. (2012), on the other hand, used a through-water Terrestrial Laser Scanning system in a field investigation to measure the bed elevation of a gravel-bed river. Using a 0.20 m deep clear water body in the laboratory, they validated this technique and reached a 5 mm accuracy. Although both techniques showed good promises to monitor morphodynamics, they have not been evaluated yet in the case of highly transient flows, as they need a steady quasi-flat free surface and the exact determination of its location (Friedl et al., 2017). Moreover, they usually require complicated setups and post-processing algorithms, or unaffordable commercial devices.

Mainly to overcome the high costs associated with the methods described hereabove, a novel approach based on modern low-range RGB image and Depth (RGB-D) sensors was developed. Initially designed for gaming platforms, these sensors are able to measure the distance to three-dimensional opaque surfaces with a high spatial resolution and at remarkable acquisition rates (30 Hz). RGB-D sensors combine both an infrared projector and camera, for distance measuring, and a digital RGB camera. In laboratory conditions, these devices have been successfully applied to the monitoring of the temporal evolution of the free water surface in case of highly unsteady flows (Martínez-Aranda et al., 2018) or to the collection of the final topography consecutive to an unsteady flow, once the flume had been completely drained (Martínez-Aranda et al., 2019). As a proof of concept, Chourasiya et al. (2017) used an RGB-D sensor to perform 3D measurements of the bed evolution under a quasi-flat surface flow. They proposed a refraction correction method for underwater measurements using a Kinect-v2 (an RGB-D sensor initially developed by Microsoft for the Xbox One game console), which is based on the time-of-fly principle, and validated this technique for a dike-breach experiment, which is a short duration process with quick changes in the bed profile. Even though RGB-D sensors are affordable, non-intrusive and need a minimal experimental setup, the 2D distance data computation is made at the hardware level, hence not available for researchers. Moreover, they also require quasi-flat water surfaces for measurements through the water surface. Besides, the spatial resolution of the infrared sensor is 640 x 480 pixels, limiting the application of this technique to large scale flume experiments. Despite the current limitations of this optical technique, it might offer the most promising alternative to capture high-resolution 2D data of transient submerged bed surfaces in the next 5-10 years.

As a proof of concept, Le Grelle et al. (2004) and Soares-Frazão et al. (2007) proposed an alternative Laser Profilometry Technique (LPT) to obtain the elevation of a submerged bed profile in a trapezoidal channel. This technique requires a simple experimental setup and different calibrations for the sub- and emerged situations, but does not apply to any camera positioning. Spinewine et al. (2004) also used LPT combined with a sweeping mirror to reconstruct in 3D the evolution of a breach growth in a sandy dike due to overtopping. No refraction correction was considered here, though. Rifai et al. (2020) improved the accuracy of that sweeping mirror LPT with a procedure coping with underwater measurements through a Direct Linear Transformation, based on sixteen calibration parameters and more than twenty control points appropriately chosen.

All the investigations and techniques discussed above highlight the need for non-intrusive, easily applicable and accurate measuring methods to detect the dynamics of submerged beds in laboratory experiments. In the literature, few sets of experimental data concern fast unsteady flows in 2D, which hinders the development of models associated with such flows. Hereunder, the LPT developed by Soares-Frazão et al. (2007) is improved to obtain non-intrusive time-resolved measurements of the submerged bed evolution caused by a dam-break flow in a channel with a 90° bend. The calibration of the technique and imaging processing needs the careful correction of the refraction caused by the air-water interface, but the process is straightforward if the relative position of the camera with respect to the laser sheet is maintained, and the experimental setup required is minimum. Eventually, the proposed method combines cheapness, simplicity, flexibility and delivers sufficiently accurate results to prove itself efficient. Furthermore, in order to validate the LPT measurements, a 3D-photogrammetric model of the drained bed surface has been performed at the end of the experiment. The obtained data have been made available for the scientific community in order to improve the calibration and validation of 2D morphological numerical models.

This paper is structured as follows: in Section 2, the laboratory flume, experiment and instrumentation are presented. Section 3 is devoted to describing the LPT data collection procedure, including the calibration and imaging processing, as well as the validation of the method. The experimental results have been reported in Section 4, where they are analysed and discussed. Finally, the conclusions are drawn in Section 5.

2. Experimental setup

The experiments were performed at the Hydraulics Unit of the LEMSC (Mechanical and Civil Engineering Laboratory, UCLouvain, Belgium). First, a description of the channel and the experimental conditions is made (Section 2.1). The instrumentation used to collect data is then described (Section 2.2).

2.1. Channel and experiment description

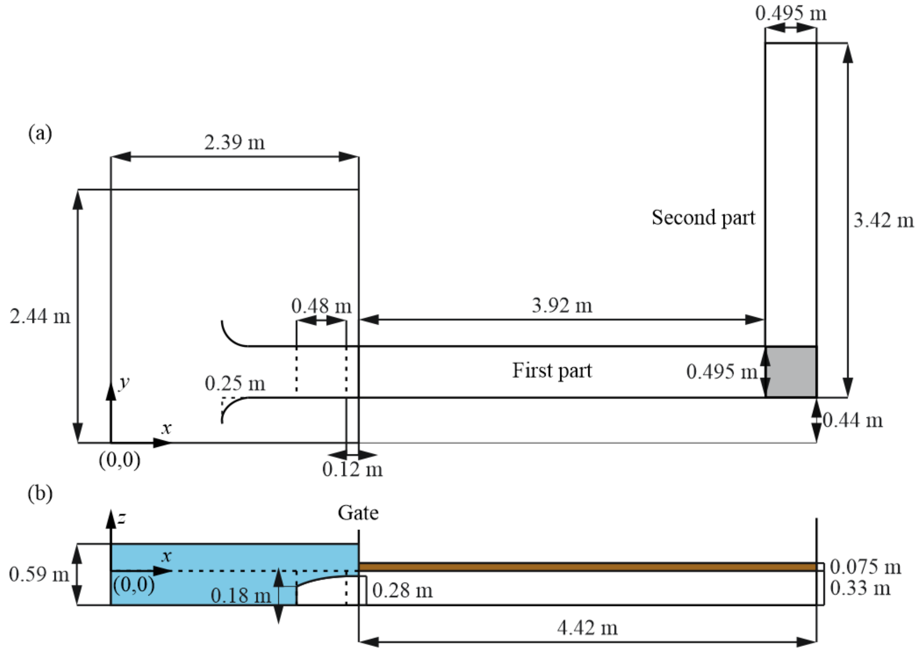

Figure 1: Channel dimensions: (a) plane view, (b) cut along the longitudinal axis of the first part of the channel.

Figure 1 1illustrates the dimensions of the channel, whose walls are made of transparent glass. An aluminium gate separates the reservoir from the channel. After 3.92 m straight, the channel suddenly turns perpendicularly. Between these two parts, the shaded square of Fig. 1a will be hereafter referred to as the bend.

A single configuration was reproduced during the whole data collection campaign. Before the gate opening, the water level rose 26 cm above the channel non-erodible bed (reference level), which was horizontal and was itself covered by a 7.5 cm high sandy layer. As explained in more detail by the preliminary study of Soares-Frazão et al. (2019), the dam-break leads to a supercritical flow until it reaches the wall opposite the gate. The flow energy then turns from kinetic to potential, which causes sediment deposition near that wall. Afterwards, the reflected water separates into a hydraulic jump going upstream and a turbulent flow heading downstream, which will progressively erode the downstream bed, and whose surface will become plain.

The sand used for the experiments can be considered as uniform and characterised by a median diameter d_{50} = 1.7 mm, a porosity ϵ_0 = 0.44 and a specific density ρ_s/ρ_w = 2.65, where ρ_s and ρ_w respectively stand for grain and water densities.

Between two experiments, a minimum waiting period of two hours was observed for the water to flow out of the channel completely. The bed material was then mixed to avoid bed compaction, especially in the first part of the channel where the shear depth was limited, and levelled manually. The reservoir was filled through a pipe at a decreasing discharge for the water to be as still as possible before gate opening.

2.2. Instrumentation

Two techniques were used to collect bed level data. The first one, LPT, on which this article focuses, combines a laser and a camera and makes it possible to monitor the bed level evolution during the experiment (Fig. 2). Photogrammetry was then used to map the equilibrium topography of the entire channel and for comparison purposes with LPT. Besides, water levels were recorded at five different positions thanks to ultrasonic gauges throughout the entire experiment.

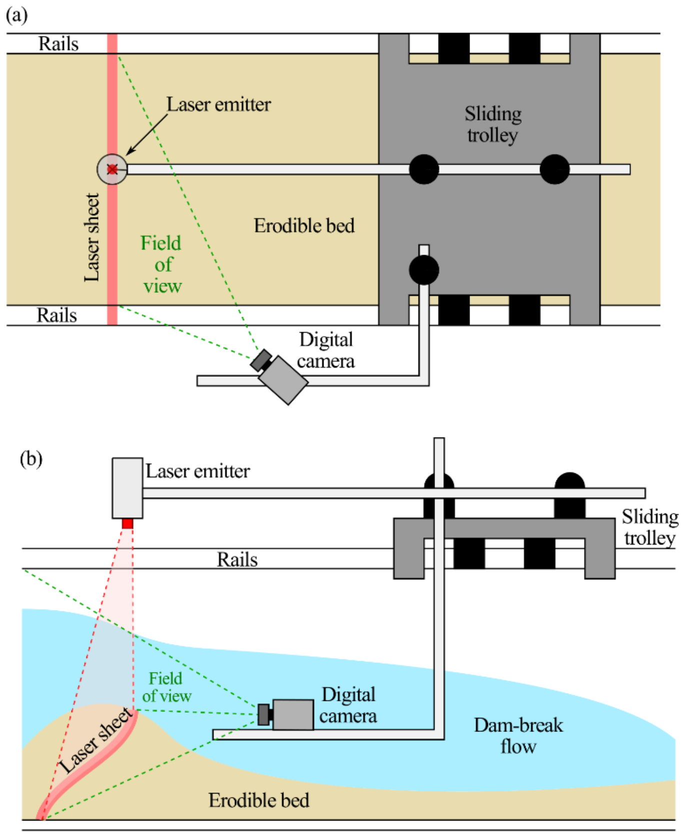

Figure 2: Top view (a) and side view (b) of the experimental setup.

The laser used for LPT was an LD-series laser from Latronix Laser Systems with a 45° opening angle. It was maintained 81 cm above reference level and projected a laser sheet either perpendicular or parallel to the flume. A monochrome Mako 131G camera from Allied Visions, powered through Ethernet, was located outside the flume. Its position was optimised by trial-and-error to remain below the water surface to avoid problems linked to its inclination, while also making sure that a significant portion of the laser kept visible during most of the experiment. Accordingly, each new relative position of the camera to the laser led to a new calibration as explained in Section 3.1. Nonetheless, for a fixed setup, as a trolley sliding on rails was used to move the whole apparatus, no re-calibration was needed from one sheet to another because the whole setup was translated. Besides, the location and orientation of the camera do not need to be known and neither do its intrinsic parameters nor the water surface elevation. Even though the coordinates of the laser profiles should be retrieved to relate the x to the z coordinates, they do not intervene in the calibration, nor in the post-treatment procedure.

At the end of the experiment, the drained bed topography was captured using a photogrammetry technique. Photogrammetry pictures were taken with a GoPro Hero 7 Silver from 6 different positions on the trolley, which was gradually and slowly slid to ensure sufficient coverage between two successive pictures. A Digital Elevation Model (DEM) was then processed thanks to Agisoft Metashape (Fig. 3). Its accuracy was estimated along 6 different cross-sections for which pointwise manual measurements were taken in an intrusive way with a 4 cm spacing between two points to avoid any influence of previous measurements (Fig. 4). The Root Mean Square Error (RMSE) between photogrammetry and the manual measurements was estimated to be 1.802 mm and 8.304 mm for the first part of the channel and the second one respectively (Fig. 5). The larger RMSE of the second part of the channel can mainly be explained by a higher manual measuring uncertainty due to the steeper local slopes. Besides, three DEMs based on three different tests were made. It appeared that the RMSE, with the error being the averaged absolute deviation of the DEM to the DEMs' mean, was equal to 3.8 mm, giving a first appreciation of the reproducibility of the experiment. Figure 6 represents the spatial variation of that error and emphasises the stronger variability of the results in the bend area and over the first fifty centimetres of part 2 where the RMSE reaches 4.7 mm.

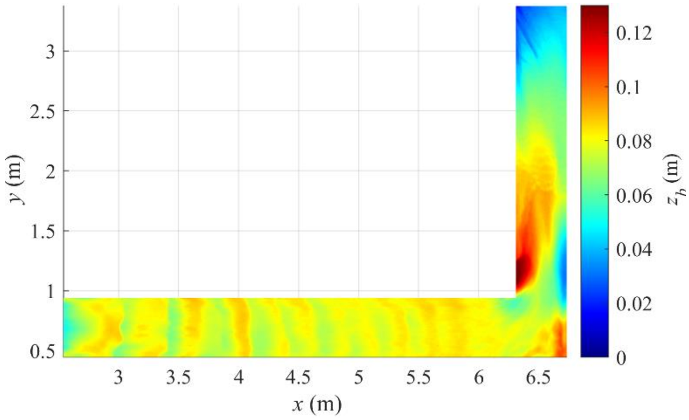

Figure 3: Final topography obtained for the third photogrammetry test case.

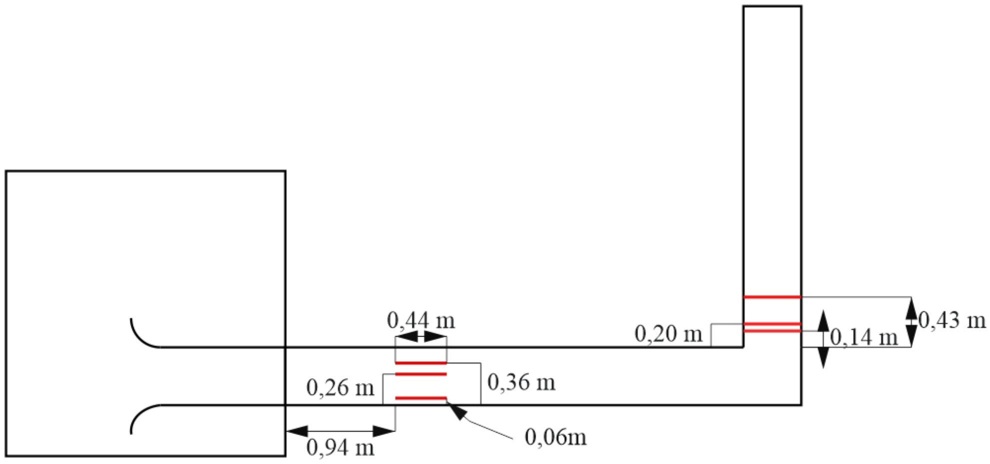

Figure 4: Positions and dimensions of the manual measurement cross sections.

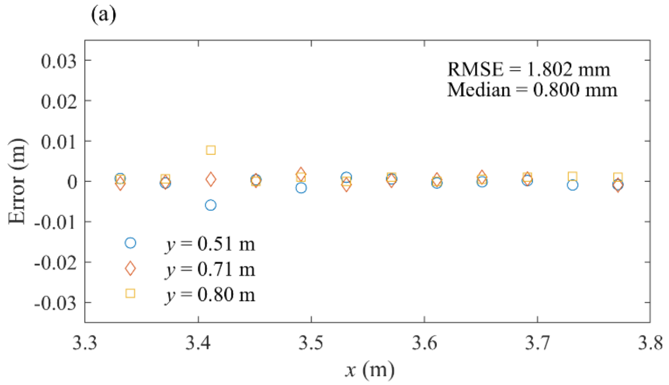

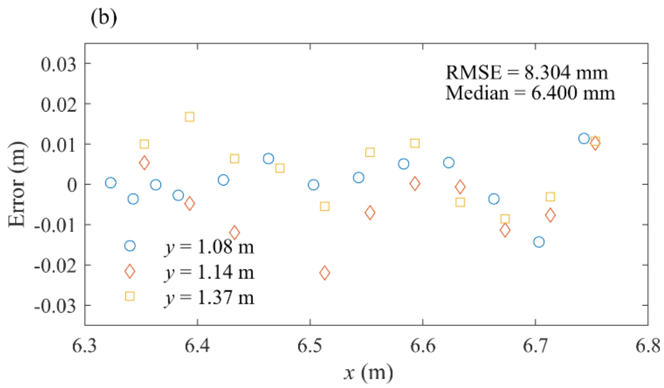

Figure 5: DEMs' deviation to the manual measurements for (a) part 1 and (b) part 2.

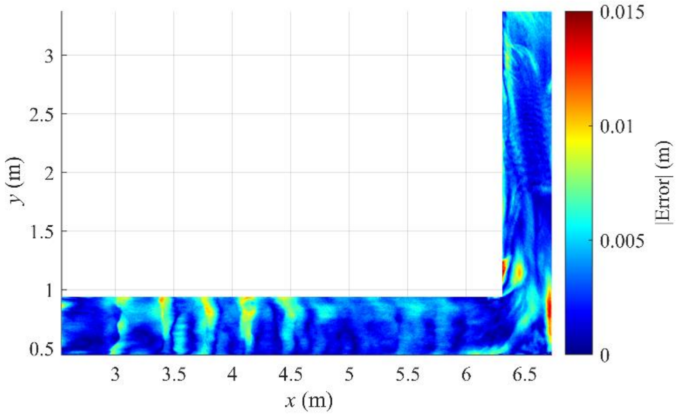

Figure 6: Averaged absolute error with respect to the DEMs' mean.

At last, water levels were collected continuously thanks to ultrasonic Baumer distance sensors (Fig. 7). Between thirty-one and thirty-four tests gave valid data for all gauges, except for gauge G4 which only admits twenty valid data sets. It was indeed impossible to set the sensor at the same place as the trolley. Once the outliers were removed, the bandwidth of the aggregated data sets associated to the different sensors varied from 9,54 mm to 22,12 mm, which gives a second estimation of the experiment repeatability. These results are attached to this paper as supplemental material.

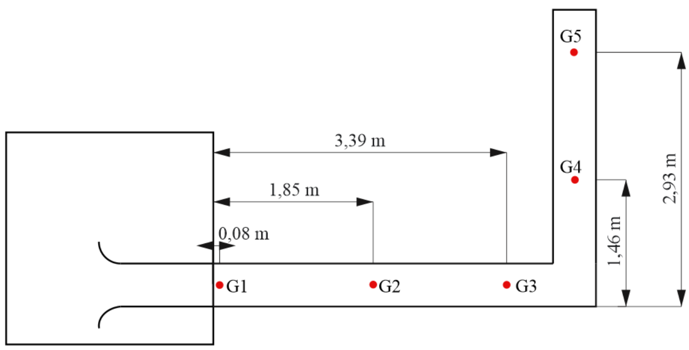

Figure 7: Positions of the water level sensors.

3. **LPT data collection procedure**

This section aims at describing the whole procedure to retrieve data with LPT. This procedure can be split into two steps: a calibration stage associated with each positioning of the camera with respect to the laser (Section 3.1) and a processing one for each experimental run (Section 3.2).

3.1. Calibration

The calibration procedure we propose here itself consists of two steps: (1) determination of the pictures' dimensions and (2) elaboration of a refraction correction linear law. Finding the best camera position by performing roughly two or three tests and going through the whole calibration procedure would generally last a full day.

Step 1 is performed thanks to a checkerboard with known dimensions that is placed upon the laser position, usually on the non-erodible bed. Positioning the checkerboard on the erodible material is possible, but requires careful levelling and an appropriate shift of the results. Using the Matlab Image Processing Toolbox (MIPT) to define a working area for future real tests, we can crop the original picture and orthorectify it (Fig. 8). Afterwards, we need to find the appropriate scaling factor that will properly convert pixels into millimetres.

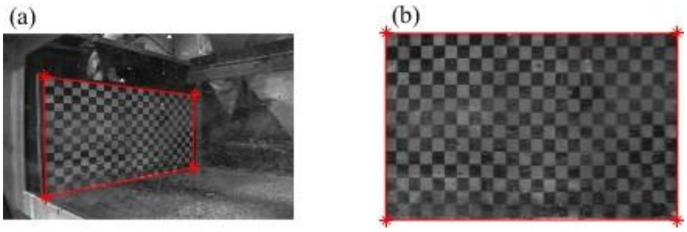

Figure 8: (a) Cropping the original picture of the calibration checkerboard, (b) orthorectification of the cropped image.

Once we made sure the dimensions measured thanks to the MIPT correspond to reality, we can reproduce step 1, but with a submerged checkerboard. Although refraction at the glass-air interface can be neglected due to the very limited thickness of the walls, it is highly likely that the widths of the underwater squares will not remain constant over the entire width of the orthorectified picture because of refraction at the water-glass interface. To fix this, we propose to simply derive a linear relation between the results obtained with the MIPT and the expected values, for the refractive index of water can be considered constant, whatever the direction of the light ray. To do so, we manually picked an arbitrary number of points for which we knew the local coordinates (Fig. 9a) and we compared them with reality (Fig. 9b). Reversing the linear equation obtained thanks to a least squares regression, we obtained a corrected series that matched almost perfectly with reality. It is also worth mentioning that modifying the elevation values is not necessary since no distortion is observed in this direction. Figure 10 shows the position of the different laser sheets for which a different calibration was made. These sheets are labelled from L1 to L5. The sheet L5, as depicted by Fig. 10, actually consists of the combination of several laser sheets retrieved from different tests, the trolley having been translated between two tests. Hereunder, referring to L5 actually concerns one sheet only, i.e. one portion of the total length of L5, if not specified otherwise.

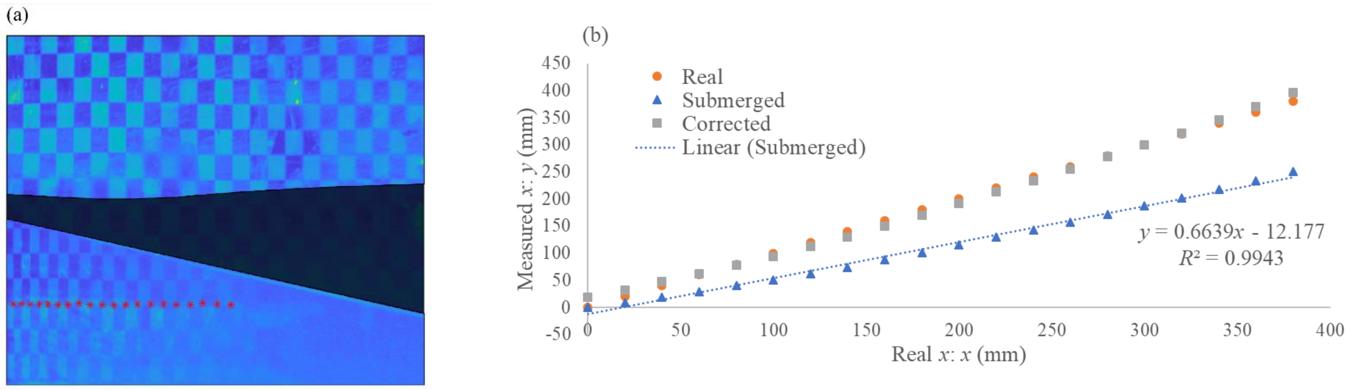

Figure 9: Calibration step 2: (a) points manual picking at the corners of submerged squares. The water surface (darkest area) separates the sub- and emerged parts of the checkerboard. (b) Determination of a linear relation between measured and real *x* coordinates. R^2 is the correlation factor.

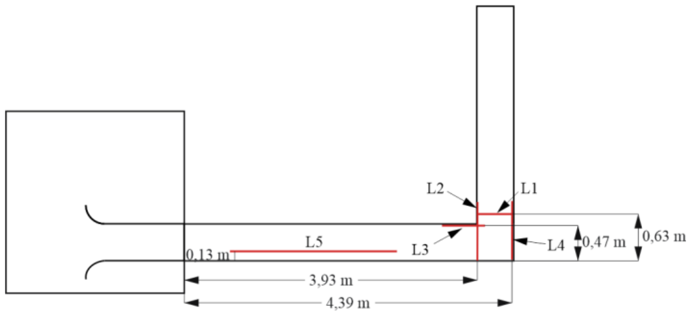

Figure 10: Location of the different examined laser sheets.

3.2. Image processing

Thanks to the linear correction law defined for each laser sheet setup, it becomes possible to treat the lasers evolving underwater. For those that stay emerged, no correction is to perform on the other hand. For a faster post-treatment of the pictures, it is advised to cover the trolley with dark sheets to better isolate the laser. An algorithm detecting the laser traces automatically, whether they are sub- or emerged, is another asset, but manual detection of the laser points with the MIPT is still an alternative if the number of images to be treated is low enough.

For all the investigated laser sheets, pictures were captured at 4 Frames Per Second (FPS) for approximately 23 s. This relatively slow acquisition rate was meant to prevent the buffer of the software from crashing. Better material could improve this frequency, though. Besides, since the camera could not always see the gate, a LED bulb linked to the gate and switched off when made opened was always set in the camera’s field of view. In this way, the last picture with the LED turned on would correspond to the last one with a closed gate. Hence, we estimate time uncertainty for the pictures to reach 0.25 s at most, which is acceptable for the purposes of the experiment and considering its duration.

The accuracy of the refraction correction was evaluated for laser sheets L1 to L5. Each time, the final dry topography was compared with the last picture for which we had an immersed insight. This last picture was taken at the end of the experiment, when no more morphological evolution of the bed could be observed by the human eye, but when the laser was still underwater though. It was thus assumed that this measured bed topography was the same as the drained topography measured by LPT without water. The RMSE between the final topography and the underwater laser profile varied from 1.25 mm to 7.28 mm, i.e. from 2.25 % to 21.14 % relatively to the final topography. The absolute RMSE always remained below 4.3 times the grain diameter, which is satisfactory. The large maximum relative RMSE corresponds to L4, located in the bend close to the wall, and is due to the low bed level over the entire sheet at the end of the experiment (of the order of 3 cm). Neither the camera angle nor its distance from the laser sheet looks to influence much the correction performance. Yet, great care should be dedicated to the determination of the different offsets between the sub- and emerged calibrations as well as to the scaling factor. A slight inaccuracy could indeed lead to strong differences between the sub- and emerged cases, especially if the considered point is far from the camera.

4. **Data analysis**

In this section, the reproducibility of the tests (Section 4.1), as well as the LPT accuracy, are assessed (Section 4.2). Finally, the underwater bed level evolution is discussed (Section 4.3).

4.1. Repeatability

Besides the global reproducibility assessment made thanks to photogrammetry results and mentioned hereabove, we compared the drained outcomes of several tests with each other for laser sheets L1 and L5 (Fig. 11). L1 and L5 envelopes were respectively made of seven and fourteen different tests. In accordance with photogrammetry RMSE results, Fig. 11 shows that sections located close to the bend were more prone to change than sections in the first part of the channel. Even though mean bandwidth and photogrammetry RMSE were not calculated similarly, the variability indication given by LPT bandwidth is in line with photogrammetric results. Anyway, if one would perform numerical simulations and compare their results with the available data, a global deviation of the order of roughly 10 mm, with some strong local deviations as well, would be expected.

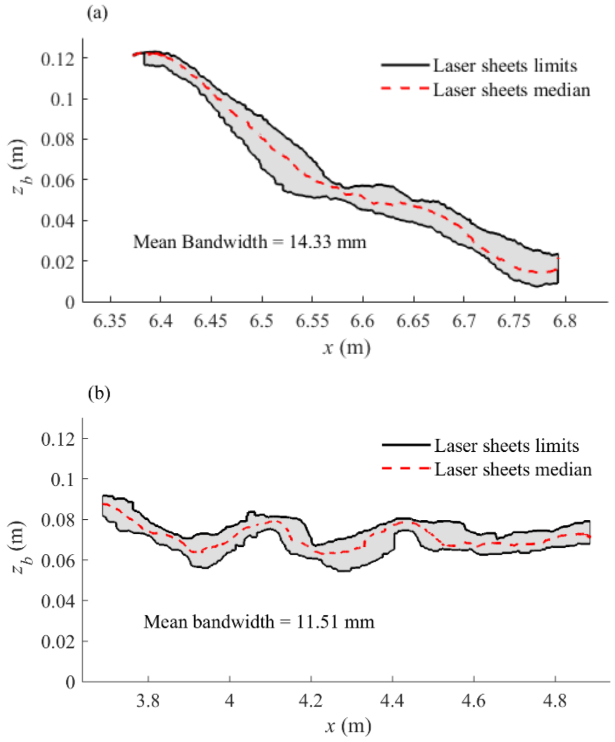

Figure 11: (a) L1 envelope, (b) L5 envelope. The moving median displayed for both figures was calculated with 300 points.

4.2. LPT accuracy

Thanks to its good precision, especially in the first part of the channel as emphasised by Fig. 5a, photogrammetry results can be used as an accurate estimation of the real bed level and can then be used for comparison purposes with LPT. For one experiment, data were recorded both with photogrammetry and LPT along the L5 laser sheet (Fig. 12a). Accordingly, the two profiles should ideally coincide. However, a noticeable spatial lag between both profiles highlights the need to measure carefully the position of the checkerboard during the calibration stage and to make sure it does not move with an appropriate stabilising system attached to it, for it can lead to a substantial error. Besides, the laser profile is somewhat lower than that of photogrammetry. Since the DEM can be considered as centred regarding the manual measurements (Fig. 5a), the RMSE between photogrammetry and LPT is a good estimation of LPT accuracy, which is actually of the same order as that obtained by Frank and Hager (2014) and Rifai et al. (2020) for steeper slopes and hence more demanding conditions, but with a more complex and expensive method. Nevertheless, LPT accuracy is highly dependent on the calibration and consequently, this RMSE value only concerns this laser sheet. In particular, it is not expected that an upwards vertical shift should always be performed to align LPT results with reality. For instance, Fig. 12b displays photogrammetry and LPT results collected for two different tests along L1. Considering the inherent variability of the experiment (see Fig. 11a), a difference between both profiles is expected, but no vertical shift looks to be required. In this case, the RMSE obtained for L5 (Fig. 12a) certainly underestimates the LPT accuracy. However, this RMSE value gives a conservative estimation of the LPT accuracy that can be expected more generally. In particular, it could be added to the error obtained in comparisons with numerical results.

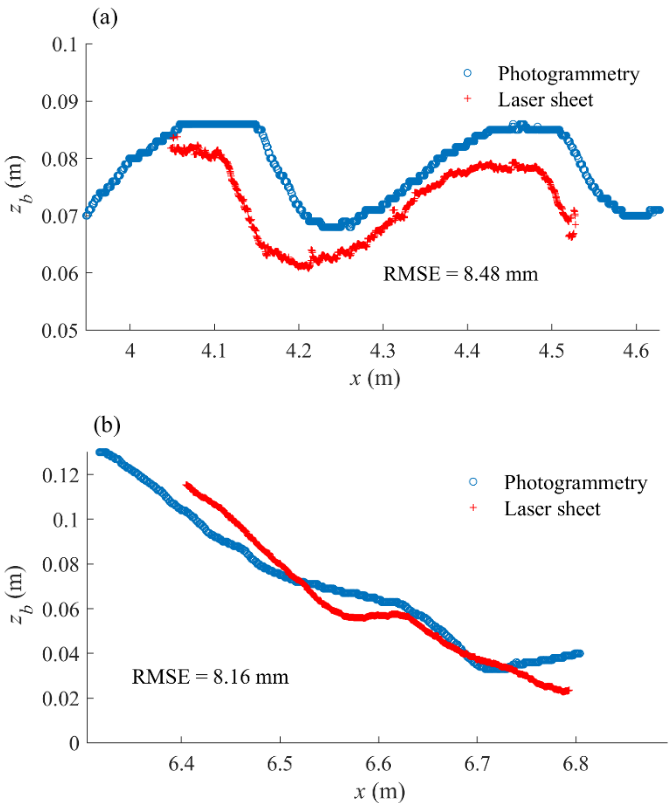

Figure 12: Comparison between photogrammetry and LPT at (a) L5 and (b) L1 cross-sections. For (a), the two techniques were used after the same test. For (b), two different tests were considered.

4.3. Bed evolution

The most appealing feature of LPT is its ability to detect underwater bed level and hence, follow its evolution when subject to a transient flow. For the considered test case, the monitoring of laser sheets L1 and L5 helped understand the most striking features of the final topography (Fig. 13).

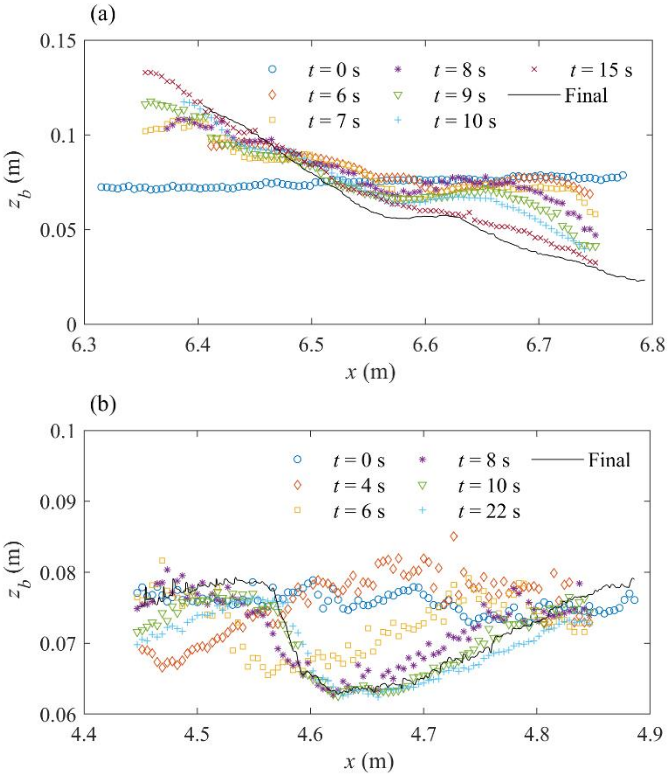

Figure 13: Bed evolution along laser sheets (a) L1 and (b) L5. Times refer to gate opening.

From Fig. 13a, different behaviours can be observed on both sides of part 2 longitudinal axis. On the left side, the sediment deposed very rapidly and the bed slope did not change much after 6 s. Yet, sediment continued accumulating for 9 s because of three-dimensional vortices at the toe of the deposit, right after the inner corner (Fig. 14). Besides vortices, the sudden deposition of sediment near the left wall at the very beginning might also be due to the sediment carried from part 1 and losing its inertia after reflecting against the wall opposite the gate, even if some had already deposed in front of that wall. Nevertheless, asserting this is difficult since the turbulence of the flow limits visibility before t = 6 s. On the right side though, scouring went very progressive as the cross-section reduced and secondary currents helped excavate some sediment near the outer bank of the flume. All these processes actually bring an answer to the poor performance of the models used by Meurice and Soares-Frazão (2020) to reproduce this test case numerically.

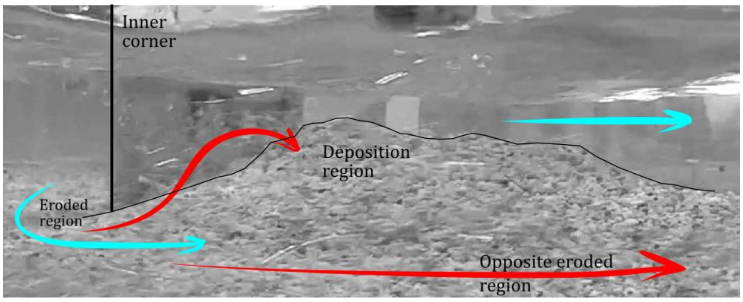

Figure 14: Shot taken after 14 s opposite the inner corner of the bend. Blue arrows indicate the water movement, while red arrows stand for the strongest sediment transport patterns. At the front, the bed gets increasingly eroded as the cross-section reduces. At the back, 3D vortices erode the bed near the inner corner and depose sediment a few centimetres higher and further downstream.

When it comes to Fig. 13b, bedforms look to have appeared and reached their full amplitude very soon after the front wave passage. As time progressed, they moved downstream, but with a decreasing pace, until they stabilised, partly due to a hydraulic jump coming from downstream and slowing down the flow.

The evolution of the bed elevation from other laser sheets is available as supplementary material and confirms the peculiar aspects of the topography evolution presented here. LPT actually proves sufficient for a qualitative analysis of the topographic history, while providing accurate results at the same time.

5. Conclusion

An upgraded version of LPT as developed by Soares-Frazão et al. (2007) was proposed to cope with refraction when monitoring underwater bed level evolution along a linear profile in laboratory models. The system only consists of a laser and a single camera and can be translated on rails without requiring a new calibration. The calibration method itself is very basic but delivers results as accurate as more complex methods do. It indeed simply consists in determining a linear relation between the observed submerged bed levels coordinates and their expected values.

The general accuracy, concerning both sub- and emerged situations does not look to be dependent either on the camera position and orientation or on the distance between the laser sheet and the camera. Nevertheless, caring for the precision of the calibration procedure is of the uttermost importance to provide accurate results.

LPT was applied to a dam-break on an erodible bed in a flume with a 90° bend for which bed and water level measurements were made available to the scientific community. It showed that the monitoring of only a few profiles was sufficient to explain the development of the most important features of the final topography. Even if the limited spatial coverage of LPT certainly constitutes a major drawback, it is also a cornerstone for the procedure's simplicity that, along with its cheapness, flexibility and good accuracy, makes it an interesting candidate for laboratory morphodynamics investigations, especially when it comes to fast transient flows.

Acknowledgements

The authors wish to acknowledge Samuel Laurent and the other technicians of the LEMSC for their help and continuous dedication to conducting the experiments as smoothly as possible.

Funding

The financial support of this research was threefold: Robin Meurice was funded as a Research Fellow of the Fonds de la Recherche Scientifique - FNRS. Sergio Martínez-Aranda was funded by the MINECO under research project PGC2018-094341-B-I00 and by Diputacion General de Aragon, DGA, through Fondo Europeo de Desarrollo Regional, FEDER. Finally, Masoumeh Ebrahimi received the support of UCLouvain as a Research Assistant.

Supplemental data

Supplemental material is available at this address: yet to determine.

Notation

d_{50} = median grain diameter (m)
ϵ_0 = bed porosity (–)
ρ_s = bed grain density (kg m^{-3})
ρ_w = water density (kg m^{-3})

References

Aberle, J., & Nikora, V. (2006). Statistical properties of armored gravel bed surfaces. *Water Resources Research, 42*(11), W11414.

Bertin, S. & Friedrich, H. (2014). Measurement of Gravel-Bed Topography: Evaluation Study Applying Statistical Roughness Analysis. *Journal of Hydraulic Engineering*, *140*(3), 269-279.

Bouratsis, P., Diplas, P., Dancey, C.L. & Apsilidis N. (2013). High-resolution 3-D monitoring of evolving sediment beds. *Water Resources Research, 49*, 977-992.

Bunte, K., & Abt, S. R. (2001). *Sampling surface and subsurface particle-size distributions in wadable gravel- and cobble-bed streams for analyses in sediment transport, hydraulics, and streambed monitoring*. Gen. Tech. Rep. RMRS-GTR-74, U.S. Dept. of Agriculture, Forest Service, Rocky Mountain Research Station, Fort Collins, CO, 1–428.

Butler, J.B., Lane, S.N. & Chandler, J.H. (1998). Assessment of DEM quality for characterizing surface roughness using close range digital photogrammetry. *The Photogrammetric Record*, *16*(92), 271–291.

Butler, J.B., Lane, S.N, Chandler, J.H & Porfiri, E. (2002). Through-Water Close Range Digital Photogrammetry in Flume and Field Environments. *The Photogrammetric Record, 17*, 419-439.

Carbonneau, P.E., Lane, S.N. & Bergeron, N.E. (2003). Cost-effective non-metric close-range digital photogrammetry and its application to a study of coarse gravel river beds. *International Journal of Remote Sensing*, *24*(14), 2837–2854.

Chourasiya, S., Mohapatra, P.K. & Tripathi, S. (2017). Non-intrusive underwater measurement of mobile bottom surface. *Advances in Water Resources, 104*, 76-88.

Cooper, J.R. & Tait, S.J. (2009). Water-worked gravel beds in laboratory flumes - a natural analogue? *Earth Surface Processes and Landforms, 34*(3), 384–397.

Dietrich, W. E., Kirchner, J. W., Ikeda, H. & Iseya, F. (1989). Sediment supply and the development of the coarse surface layer in gravel-bedded rivers. *Nature, 340*(6230), 215–217.

Frank, P.-J. & Hager, W.H. (2014). Spatial dike breach: Accuracy of photogrammetric measurement system. *Proceedings of River Flow 2014, Lausanne, Switzerland*.

Friedl, F., Schneider, J., Hinkelammert, F. & Weitbrecht, V. (2013). Through-water terrestrial laser scanning in hydraulic scale models: proof of concept. *Journal of Hydraulic Research, 56*(4), 551-559.

Goring, D.G., Nikora, V.I. & McEwan, I.K. (1999). Analysis of the texture of gravel-beds using 2-D structure functions. *Proceedings of IAHR. Symp. on River, Coastal and Estuarine Morphodynamics 1999, Genova, Italy*.

Henning, M., Hentschel, B. & Husener, T. (2008). Determination of channel morphology and flow features in laboratory models using 3D-photogrammetry. *Proceedings of River Flow 2008, Izmir, Turkey*.

Le Grelle, N., Spinewine, B., Soares-Frazão, S. & Zech, Y. (2004). Non-intrusive imaging measurements of the morphological evolution of a channel during a dam-break flow. *Proceedings of River Flow 2004, Napoli, Italy*.

Martínez-Aranda, S., Fernández-Pato, J., Caviedes-Voullième, D., García-Palacín, I. & García- Navarro, P. (2018). Towards transient experimental water surfaces: A new benchmark dataset for 2D shallow water solvers. *Advances in Water Resources, 121,* 130-149.

Martínez-Aranda, S., Navas-Montilla, A., García-Palacín, I. & García-Navarro, P. (2019). 2D non- intrusive measurements of dam-break waves in channels with movable bed and width variations. *Geophysical Research Abstracts, 21*, 1-1.

Meurice, R. & Soares-Frazão, S. (2020). A 2D-HLL based weakly coupled model for transient flows on mobile beds. *Journal of Hydroinformatics, 22*(5), 1351-1359.

Rifai, I., Schmitz, V., Erpicum, S., Archambeau, P., Violeau, D. (...), El Kadi Abderrezzak, K. (2020). Continuous monitoring of fluvial dike breaching by a Laser Profilometry Technique. *Water Resources Research, 56*(10).

Smith, M., Vericat, D. and Gibbins, C. (2012). Through-water terrestrial laser scanning of gravel beds at the patch scale. *Earth Surf. Process. Landforms, 37*, 411-421.

Soares-Frazão, S., Le Grelle, N., Spinewine B. & Zech, Y. (2007). Dam-break induced morphological changes in a channel with uniform sediments: measurements by a laser-sheet imaging technique. *Journal of Hydraulic Research, 45*:sup1, 87-95.

Soares-Frazão, S., Abbeels, S. & Messens, M. (2019). Dam-Break Flow in a Channel with a 90° Bend and Mobile Bed: Experimental and Numerical Simulations. *Proceedings of the 38th IAHR World Congress, Panama City, Panama.*

Spinewine, B., Delobbe, A., Elslander, L. & Zech, Y. (2004). Experimental investigation of the breach growth process in sand dikes. *Proceedings of River Flow 2004, Napoli, Italy*.

List of figures

Figure 8 (a) Cropping the original picture of the calibration checkerboard, (b) orthorectification of the cropped image.

Figure 9 Calibration step 2: (a) points manual picking at the corners of submerged squares. The water surface (darkest area) separates the sub- and emerged parts of the checkerboard. (b) Determination of a linear relation between measured and real x coordinates. R^2 is the correlation factor.

Figure 10 Location of the different examined laser sheets.

Figure 11 (a) L1 envelope, (b) L5 envelope. The moving median displayed for both figures was calculated with 300 points.

Figure 12 Comparison between photogrammetry and LPT at (a) L5 and (b) L1 cross-sections. For (a), the two techniques were used after the same test. For (b), two different tests were considered.

Figure 13 Bed evolution along laser sheets (a) L1 and (b) L5. Times refer to gate opening.

Figure 14 Shot taken after 14 s opposite the inner corner of the bend. Blue arrows indicate the water movement, while red arrows stand for the strongest sediment transport patterns. At the front, the bed gets increasingly eroded as the cross-section reduces. At the back, 3D vortices erode the bed near the inner corner and depose sediment a few centimetres higher and further downstream.